Available online at www.sciencedirect.com
SCIENCE DIRECT®
European Polymer Journal 41 (2005) 2803–2823
EUROPEAN POLYMER JOURNAL
www.elsevier.com/locate/europolj

Review

Characterization of adhesion at solid surfaces: Development of an adhesion-testing device

Attila Oláh, G. Julius Vancso *

Department of Materials Science and Technology of Polymers, MESA+ Institute for Nanotechnology, Faculty of Science and Technology, University of Twente, P.O. Box 217, 7500 AE, Enschede, The Netherlands
Dutch Polymer Institute, P.O. Box 902, 5600 AX, Eindhoven, The Netherlands

Received 28 March 2005; received in revised form 8 June 2005; accepted 8 June 2005
Available online 2 August 2005

Abstract

A custom-built adhesion-testing device (ATD) is described in this paper, which was developed to study energetics of various solid (polymeric) interfaces. A review is also given of the main techniques of adhesion and adherence measurements, including non-destructive and destructive methods, with major emphasis on the evolution and applications of contact mechanics techniques. Using the Johnson–Kendall–Roberts (JKR) theory of contact mechanics in the elastic deformation regime, the interfacial energy of solid surfaces can be obtained by measuring the contact radius, loading force, and vertical displacement between an (elastic) sphere (lens) and a flat surface (one of which, or both, coated with the sample of interest). The parameters needed for JKR analyses were determined by our custom-built device. Based on the JKR theory, the values of work of adhesion, combined elastic modulus and interfacial energy were determined from the loading and unloading curves on poly(dimethylsiloxane)–poly(dimethylsiloxane) (PDMS) systems. Cumulative adhesion hysteresis and elastic modulus were also calculated. The results obtained agree well with literature data measured by different methods. These measurements on compliant PDMS–PDMS model systems can also serve as validation and verification of the adhesion-testing devices described in this study.

Keywords: Adhesion; JKR; Poly(dimethylsiloxane); Contact mechanics

Contents

* Corresponding author. Address: Department of Materials Science and Technology of Polymers, MESA+ Institute for Nanotechnology, Faculty of Science and Technology, University of Twente, P.O. Box 217, 7500 AE Enschede, The Netherlands. Tel.: +31 53 4892967; fax: +31 53 4893823.
E-mail address: g.j.vancso@utwente.nl (G.J. Vancso).

0014-3057/$ - see front matter © 2005 Elsevier Ltd. All rights reserved.
doi:10.1016/j.eurpolymj.2005.06.008

1. Introduction

From a practical point of view, adhesion tests are developed to characterize adhesives and adhering joints. According to Tod [1] the main objectives of adhesion tests are: (i) quality check of an adhesive, (ii) determination of the effectiveness of a surface pretreatment, (iii) prediction of a joint performance (data collection), (iv) selection of an adhesive for a specific application, and (v) evaluation of the effect of ageing. Considering the versatility of adhering materials, geometries and requirements for adhesive joints, it is obvious that a universally applicable adhesion-testing method cannot be developed. It must be emphasized that the adhesion phenomenon originates from surface forces acting between various surfaces. Therefore, surface forces are of utmost importance for the understanding of adhesion phenomena and for determining the behavior of interfaces. To date, many techniques have been developed and are available for direct characterization of surface forces and adhesion phenomena. In general, these methods can be classified as destructive and non-destructive measurements [2]. Using destructive methods, sizable parts of specimens under investigation undergo large deformations. Therefore, bulk viscoelastic properties strongly influence the value of adhesion measured. As a consequence of the large deformations, there is always a viscoelastic energy loss, which is hard to deconvolute from the results. It must be pointed out here that the adhesion data obtained by both destructive and non-destructive methodologies is also dependent on the measurement conditions such as the rate, temperature and humidity of testing. Destructive adhesion tests always employ solid bodies and the main three commonly used test configurations include tensile, peel, and shear experiments.

The importance of the intermolecular interactions between surfaces such as solids, dispersions, emulsions, lipid bilayers and foams has been realized for a long time. In order to understand the theoretical background, and to study the effects of surface forces of such systems, various techniques and methods have been developed. The most common test is the wetting method, which indirectly characterizes the surface tension of the surfaces utilizing contact angle measurements [3–8]. This technique uses a series of test liquids to estimate the surface energy of the substrate. However, specific interactions between the liquid and the solid surface can influence the values of the contact angles measured. Despite of the deficiencies, the wetting method is widely applied in surface characterizations. The inverse gas chromatography (IGC) technique is also used in characterization of surface and surface energetics, but mainly for powders [9]. The results of IGC measurements are primarily useful for comparing materials. The first successfully used instrument to directly measure forces acting on a surface was the surface forces apparatus (SFA) [10–12]. The apparatus was designed and built by Tabor and Winterton [10]. Later it was further developed by Israelachvili and Tabor [11] and by Israelachvili and Adams [12]. Forces by this device are measured between two appropriately shaped, smooth mica surfaces, one of which (or booth) can be coated by a material to be studied. The SFA apparatus utilizes an interferometer to follow the separation of the smooth mica surfaces, while the forces are calculated from the deflection of a leaf spring. Limitations of the SFA approach include that (i) the samples must be transparent, (ii) the surfaces studied must be smooth over a large area, and (iii) the additional mica-sample interface makes the analysis often complicated [13].

Direct solid–solid surface characterization can be performed by specially designed instruments measuring contact forces, separation and contact areas between two surfaces (e.g. a lens and flat) [14]. The design of this device is inspired by the JKR contact mechanics [14] and will be called hereafter as adhesion-testing device (ATD).

In the original work of Johnson–Kendall–Roberts the adhesion was measured between two contacting spherical rubber surfaces and between polyisoprene and poly(methyl methacrylate) contacting sphere and flat pairs. JKR instruments usually utilize an optical microscope to measure the contact area between a spherical cap (lens) and a flat substrate (or a lens). In the measurement the lens is pressed against the flat substrate (or lens), and it is subsequently retracted until separation occurs. Under the imposed displacement (d), the contact area (a) and the external load (P) are recorded. Using the measured values of a and P, values of the work of adhesion can be determined between the contacting surfaces by the JKR theory. Although the basic principles of the device and the measurement remained the same, the instrumentation has significantly developed through the years [15–18]. The JKR technique requires that one of the contacting surfaces is optically transparent (or opaque) and the other should be compliant (or a combination of these).

The most widespread surface force characterization technique nowadays is the atomic force microscope (AFM), also known as scanning force microscope (SFM) [19,20]. Since the invention of AFM a great number of techniques have been developed as variations of the original contact mode design, and the scope has broadened enormously [21]. This technique, which employs a cantilever-mounted "ultra" sharp tip, a piezoelectric micropositioner, a cantilever deflection sensor, and a feedback mechanism for the positioner, was first used mainly for surface imaging [20]. However, later, using the force-sensing capacity of the AFM, it was also applied in surface force measurements i.e. measuring forces between the tip and the sample vs. their separation distance. Although such force–distance curves obtained are often difficult to interpret due to the lack of knowledge of the exact contact geometry, usually the JKR theory of contact mechanics is used to estimate surface forces and the adhesion also by AFM [21].

Other techniques, such as the so-called measurement and analysis of surface interaction force apparatus (MASIF) [22,23], thin-film-balance [24–27], osmotic stress method [28–30], interfacial force microscopy [31], and optical tweezers [32–35] have been developed for studying surface forces. These techniques also contributed to a deeper understanding of surface forces and adhesion phenomena for various interfaces.

In this paper first some of the main techniques of surface force measurements on solid surfaces are discussed; i.e. a general overview of the destructive adhesion measurements, the wetting method, SFA, AFM, MASIF, and JKR-like techniques is given. The basic principles of these techniques will be explained with a special focus on the milestones of the development of the ATD measurement techniques. Subsequently, we describe in detail our custom-built adhesion device, which has been used in studies of various solid interfaces [36,37].

1.1. Destructive adhesion measurements

The term adhesion is used for the fundamental atomic and molecular forces responsible for holding two phases together. However, the quantities coming from destructive tests of adhesion such as the peel strength, are also widely referred to as adhesion. This quantity, representing a sum of the work of (thermodynamic reversible) adhesion, combined with dissipative energy losses related to various physical and chemical factors, etc., is referred as adherence in this paper.

Destructive tests are traditionally used to investigate adherence of adhesives (joints) or coatings, however the results of these measurements primarily reflect the mechanical response of the interface in combination with the theoretical work of adhesion [2]. Thus, information obtained is primarily related to the practical performance of the tested materials. Through the years a number of experimental tests have been standardized (ISO, ASTM, etc.). Well-established and widely used tests include (i) peel tests including peel at 90° and 180°, T-peel, climbing drum, floating drum, tape-test, etc.; (ii) fracture and impact resistance tests; (iii) tensile or compression tests (axially load) of butt joints and various layouts of lap joints; (iv) shear torsion; (v) shear fatigue; (vi) blister test; and (vii) cleavage [1].

Several attempts have been made to decouple the thermodynamical work of adhesion from the rheology of joint and to interpret the related phenomena of adhesive and cohesive failure by destructive tests [2,38]. Some theories of fracture processes have been developed to analyze mathematically the load values at which the cracks propagate and describe the manner in which they grow [39]. The two main approaches are the fracture mechanics using the stress intensity factor [40] and the energy-balance approach using the strain energy release rate [41].

The most common test method used to describe the performance of flexible joints is the peel test. The basic layouts for the corresponding experiment can be seen in Fig. 1. Using the energy-balance approach, if a 90° peel of an inextensible strip is considered (Fig. 1a) the peel energy P (also called peel strength) is given as [2]:

$$P = F/b = W_a \ [\text{or } W_c] + \Psi_{plast} + \Psi_{v/e} + \Psi_{bend} \qquad (1)$$

where F is the measured peel load, b is the width of the strip, and W_a and W_c are the work of adhesion and cohesion, respectively. The rheology is included by means of the term of energy dissipation Ψ, which is the sum of Ψ_{plast} (plastic deformation), $\Psi_{v/e}$ (viscoelastic loss), and Ψ_{bend} (bending).

The crack propagates (i.e. the peeling proceeds) if the amount of the work of fraction per unit area (G) reaches, or exceeds, the value of the critical strain energy release rate (G_c), which is also known as adhesive fracture energy. For a general peel test (Fig. 1c) the value of G_c is given as:

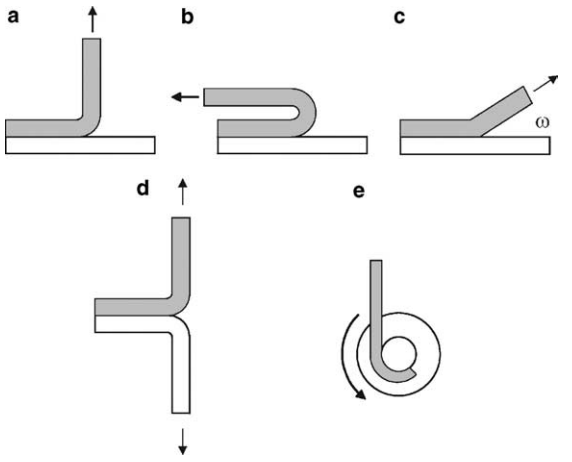

Fig. 1. Different types of peel tests. (a) 90° peel, (b) 180° peel, (c) general layout, (d) T-peel, and (e) climbing drum [2].

$$G = P(1 - \cos\omega) \geqslant G_c \tag{2}$$

Similar to the peel energy P in Eq. (1) the G can be expressed as the sum of energy and energy dissipation terms:

$$G = W_a \text{ [or } W_c] + \Psi \tag{3}$$

Similar approaches can be used for the other destructive tests, as well. The main disadvantage of the destructive adhesion tests is that the interface is irreversibly destroyed. A further challenge is that the results obtained depend on the test parameters [1]. For instance the values acquired are mainly influenced by the test rate and the temperature because of the effect of viscoelasticity [42]. Thus the glass transition temperature of the adhesive becomes a key parameter in these measurements. Another important parameter is the thickness of the adhesive within an adhesive joint, since essentially the energy dissipation takes place within this layer [1]. Many tests, for example tensile and shear tests, measure a critical stress rather than the energy value of the energy of fracture [43]. Therefore the destructive tests reflect the rheology of the joint more than the surface energy or the work of adhesion. Both rheology of joints and fundamental interfacial forces contribute to the data measured by the destructive tests, and both determine the loads under which the joint will fail in service.

1.2. Non-destructive measurements

These methods are primarily used for the determination of thermodynamic work of adhesion. In this section some of the main techniques are listed with special emphasis on the adhesion-testing device development.

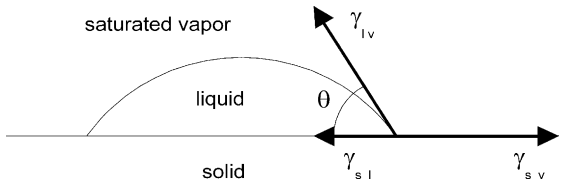

Fig. 2. Schematic of contact angle of a liquid on a solid. γ_{sl}, γ_{sv}, and γ_{lv} are the solid–liquid, solid–vapor, and liquid–vapor interfacial tensions, respectively.

1.2.1. Contact angle measurements

Contact angle measurements have been used extensively to estimate surface energy of a solid. The general layout of a contact angle between a solid and a liquid is depicted in Fig. 2.

The solid–liquid equilibrium can be stable or metastable [38]. Stable equilibrium can be achieved if the surface of the solid is ideally smooth and homogeneous, planar and non-deformable. Metastable equilibrium can occur if the surface of the solid is rough or heterogeneous. The metastable contact angle depends on the droplet size, advancing (θ_a) or receding (θ_r) state of the droplet, and mechanical perturbations. The difference between θ_a and θ_r is called contact angle hysteresis. If it exists, its value can refer to a rough or chemically heterogeneous surface, as well as to interactions between the solid surface and the probe liquid [38].

The surface tension (γ_s) of solid polymers is usually characterized by known reference liquids [44]. Assuming the interfacial tension between the liquid–vapor (γ_{lv}) to be known, measurements of the equilibrium contact angle θ lead to the difference between the solid–vapor (γ_{sv}) and solid–liquid (γ_{sl}), surface tension values according to the Young–Dupré equation, which is given as:

$$\gamma_{lv}\cos\theta = \gamma_{sv} - \gamma_{sl} \tag{4}$$

The surface energy of a solid cannot be simply determined from this equation, since γ_{sv} and γ_{sl} cannot be evaluated separately without additional information. Furthermore, the value of γ_{sv} is not equal to γ_s. The spreading pressure (π_e) gives relation between them:

$$\pi_e = \gamma_s - \gamma_{sv} \tag{5}$$

However, the value of π_e is negligible when the contact angle is below 10°. In order to estimate the surface energy of solids from experimental data several models have been developed. These models usually apply if certain simplifications are considered.

The Zisman's plot is one of the most frequently used approach for surface tension determination [3]. The principle was to measure contact angles of a series of liquids of decreasing surface tension on the solid material of interest. Zisman and coworkers also introduced the concept of critical surface tension (γ_c) [3]. This empirical quantity is defined as the value of γ_{lv} at the intercept of

$\cos\theta$ vs. γ_{lv} with the horizontal line, $\cos\theta = 1$. The estimated surface energy is written as:

$$\gamma^{\Theta}_{\text{Zisman}} = \gamma_c = \lim_{\theta\to 0}\gamma_{lv} \tag{6}$$

where the value of $\cos\theta$ varies with γ_{lv}. A drawback of this equation is that the predicted value of γ_c depends on the probe liquids and is not universally valid.

The Good–Girifalco–Fowkes' (GGF) equation was developed to improve the shortcomings of the Zisman analysis. The Zisman's plot takes neither the solid–liquid interaction, nor the difference in interactions between the solid surface and different probe liquids into account. The first model to account for the solid–liquid interaction is the GGF equation, which is based on the so-called Berthelot's relation [45] for constants expressing the attraction [4,5]. The GGF equation is valid only when the solid–liquid interactions are dominantly dispersive. Using:

$$\gamma_{sl} = \gamma_{sv} + \gamma_{lv} - 2\Phi\sqrt{(\gamma_{sv}\gamma_{lv})} \tag{7}$$

in Young's equation leads to:

$$\frac{(1+\cos\theta)}{2} = \Phi\sqrt{\frac{\gamma_{sv}}{\gamma_{lv}}} \tag{8}$$

where the Φ is the Good–Girifalco parameter, which can be determined if the chemical constitution of the surface is known. When the solid–liquid interactions are predominantly dispersive, $\Phi \to 1$ the surface energy (γ^{e}_{GGF}) can be obtained from the plot of $\cos\theta$ vs. $\gamma_{lv}^{-0.5}$, which is known as the Good–Girifalco–Fowkes' plot. Mangipudi [13] tested solid polymer surfaces using various probe liquids and reached the following conclusions: (i) the value of Φ depends more on the probe liquid than on the nature of the solid surface, (ii) using liquids with predominant dispersive interactions Φ is close to unity (London dispersive forces are dominant), (iii) Φ is small if the association effects of the probe liquid (water, formamide, etc.) due to H-bonding are dominant, and (iv) the value of Φ is moderate when the molecular size of the probe liquid is relatively large (larger than water). Mangipudi also noted that the value of Φ increases as the molecular size of the probe liquid increases. This means that as the molecular size increases, the contribution of dispersion interactions to the total intermolecular forces increases.

Wu's equation of state is a series expansion of GGF equation [6]:

$$\gamma_{c,\Phi} = \Phi^2\gamma_s - \pi_e = \frac{(1+\cos\theta)^2\gamma_{lv}}{4} \tag{9}$$

The value of the corresponding surface tension γ^{e}_{Wu} is the maximum of the plot of $\gamma_{c,\Phi}$ vs. γ_{lv}. The advantage of Wu's equation is that it accounts for solid–liquid interactions, though only qualitatively.

The geometric mean approximation, proposed by Wu [7], is an extension of the GGF equation. This approach is necessary to compensate for the deficiency of GGF which predicts a significantly higher value for γ_s than the critical surface tension where γ_s is predicted significantly higher than the critical surface tension. Dispersive and polar components of solid surface energy are calculated by solving the following equation:

$$\gamma_{lv}(1+\cos\theta) = 2\sqrt{\gamma_s^d\gamma_{lv}^d} + 2\sqrt{\gamma_s^p\gamma_{lv}^p} \tag{10}$$

The harmonic mean approach [8] is similar to the geometric mean approximation. In this approach the surface energy of the solid can be calculated by solving the following equation:

$$\gamma_{lv}(1+\cos\theta) = 4\frac{\gamma_s^d\gamma_{lv}^d}{\gamma_s^d+\gamma_{lv}^d} + 4\frac{\gamma_s^p\gamma_{lv}^p}{\gamma_s^p+\gamma_{lv}^p} \tag{11}$$

The values of surface energies and work of adhesion calculated by means of the aforementioned theories are reasonably correct and widely used [46]. However, all these methods employ questionable simplifications. The most frequently questioned simplifications are the following [46,47]:

- In the basic approach of the work of adhesion the spreading pressure π_e is included, which is generally assumed to be zero.
- The critical surface tension, γ_c, is also questioned to be a characteristic quantity of the surface.
- The value of the GGF interaction parameter Φ is usually made equal to unity. However, other approaches claim that the surface energy is a sum of the acting forces at an interface.
- The geometric and the harmonic means use the concept of polar components. This is suggested to be replaced by acid–base interaction parameters.

1.2.2. Inverse gas chromatography

Powder particles are a special type of solid bodies due to their small size, often broad size distribution, and usually irregular surface topography. For the investigation of their surface characteristics a unique technique, the inverse gas chromatography (IGC), can be used. In practice, the IGC measurements are carried out in a similar manner as traditional gas chromatography measurements, though in the case of IGC the stationary phase (powder) is the subject of interest [48]. The interactions between the eluent and the stationary phase influence the shape and the elution time of the chromatogram. Theoretical work of adhesion (W_a) can be obtained by using the following equation [49,50]:

$$W_a = 2(\gamma_1^d\gamma_2^d)^{1/2} + n^{ab} f\,\Delta H_A^{ab} \tag{12}$$

where f is a chromatography correction factor, n^{ab} is the number of interacting acid–base sites at the surface of

the sample of interest, ΔH_A^{ab} is the enthalpy related to acid–base interaction, and γ_1^d and γ_2^d are the dispersive components of the surface tension of phases 1 and 2, respectively. If only secondary forces are acting between the sample and the eluent, the value of W_a can be determined from the free enthalpy of adsorption and the net retention volume. Two alternative approaches have been worked out for the calculations. The fist approach is given as [48,51]:

$$RT \ln V = 2N(\gamma_s^d)^{1/2} a_{LV} (\gamma_{LV}^d)^{1/2} + C \tag{13}$$

where γ_{LV}^d is the surface energy of the probe, V is the net retention volume, and C is a selected reference state dependent constant.

The second approach is given as [52]:

$$-RT \ln \frac{V}{V_{n+1}} = 2N(\gamma_s^d)^{1/2} a_{CH_2} (\gamma_{CH_2})^{1/2} \tag{14}$$

where N is the Avogadro number, V_n and V_{n+1} are the retention volumes of n-alkanes with n and $n+1$ atoms, respectively, a_{CH_2} is the surface area occupied by a $–CH_2–$ group, and γ_{CH_2} is the surface tension of the polymer.

In case of acid–base interactions between the adsorbate and the adsorbent the value of ΔH_A^{ab} can be determined by the following equations:

$$\Delta G_A^{ab} = -RT \ln \frac{V}{V_r}, \quad \Delta G_A^{ab} = \Delta H_A^{ab} - T \Delta S_A^{ab} \tag{15}$$

where ΔG_A^{ab} is the acid–base part of the free enthalpy of adsorption, V_r is the retention volume, and ΔS_A^{ab} is the entropy of acid–base interaction of the components. The value of ΔH_A^{ab} can be obtained from the slope of $\Delta G_A^{ab}/T$–$1/T$ plots. The other method derives the value of ΔH_A^{ab} from the acid–base parameters of the components [51,53,54]:

$$\Delta H_A^{ab} = K_A DN + K_D AN \tag{16}$$

where the K_A and K_D are constants characterizing the acidity and basicity of the solid surface, and DN and AN are the acceptor and donor numbers of the probe, respectively.

A disadvantage of the IGC technique is that the results obtained on materials exhibiting high-energy surfaces are sensitive to the pretreatment of the sample e.g. water content, as well as to the measurement conditions [55]. Therefore, the determined surface characteristics of these materials are influenced by the circumstances of sample preparation procedure and measurement conditions. In order to obtain appropriate and comparable data the measurements should be performed under similar (or standard) conditions.

The IGC technique has been used to characterize the surface characteristics of $CaCO_3$ fillers of polymer systems [55], mineral oxides [56,57], polymeric materials [58], polymer impregnated inorganic materials [59], toner particles [60], among others.

1.2.3. Surface forces apparatus

Based on the work of Derjaguin and coworkers [61,62], Tabor and Winterton built the so-called surface forces apparatus (SFA) in 1969 [10]. The basic requirements they set were the application of smooth surfaces (mica), accurate measurement of the separation (multiple beam interferometry), and sensitive measurement of the attractive forces. The specimens used were two cylindrically bended and crossed mica sheets, which were attached to a leaf spring and a piezoelectric device. The force acting between the mica surfaces was measured with a sensitivity of 10^{-8} N. The apparatus utilized a metal spring and a pivoting arm to which the mica cylinders were attached. During measurement the pivoting arm (leaf spring) was rotated upwards coarsely by a screw thread. The fine adjustment was carried out by means of a piezoelectric transducer. In these experiments the deflection of the measuring spring due to attractive forces was studied and the surface force could be calculated using the value of the spring constant. Later the SFA apparatus was refined by Israelachvili and Tabor [11], then by Israelachvili and Adams [12].

Typical contemporary constructions utilize an interferometer to follow the separation of the cylindrically bended (radius ~1 cm) and crossed mica sheets (Fig. 3). At the surfaces of thin (2–3 μm) mica sheets the molecules of interest can be deposited or adsorbed. By measuring the wavelengths of fringes of equal chromatic order (FECO) the film thickness of material on the mica, the separation distance between the surfaces, and the radius of curvature can be determined with a resolution of 0.1 nm (Fig. 4) [63,64]. The distance between the mica surfaces is controlled by the use of (i) coarse control by the upper rod (~50 nm), (ii) medium control by the lower rod (0.1 nm), and (iii) piezoelectric tube (0.1 nm) (Fig. 3). The force acting between the samples is measured by a single or double cantilever spring, which have stiffness as that can be adjusted during the experiment. The interaction force can be calculated by applying Hook's law ($F = k\Delta x$), i.e. multiplying the spring constant (k) and the distance difference between the piezodisplacement and the sample separation (Δx). The sensitivity of the force measurement is better than 100 nN in favorable conditions. Using SFA force–distance curves, values of pull-off force, contact radius (from the shape of the FECO fringes see Fig. 4a and b), and radius of mica curvature can be obtained. The measurements can be carried out in liquids or vapors. Limitations of the SFA measurement include that (i) the samples need to be transparent, (ii) surfaces need to be smooth over a large area, and (iii) the additional mica–sample material interface makes the analysis complicated [12].

It must be pointed out, that the use of the SFA apparatus is not restricted to surface force measurements. The development of the SFA expanded its application

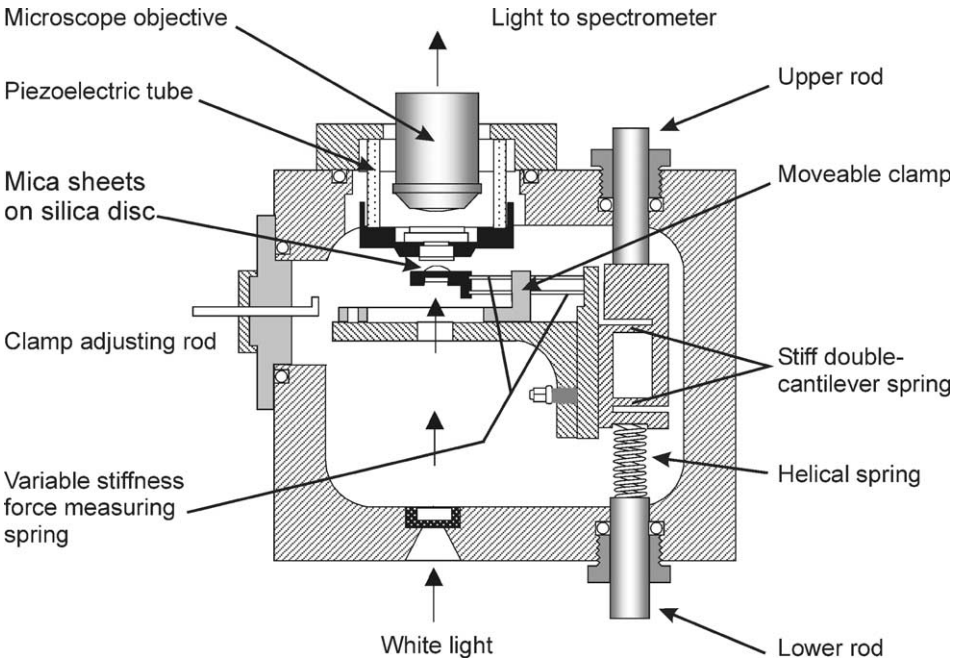

Fig. 3. Schematic showing the surface forces apparatus. (Reproduced from [63], Copyright (2005), with permission from Elsevier.)

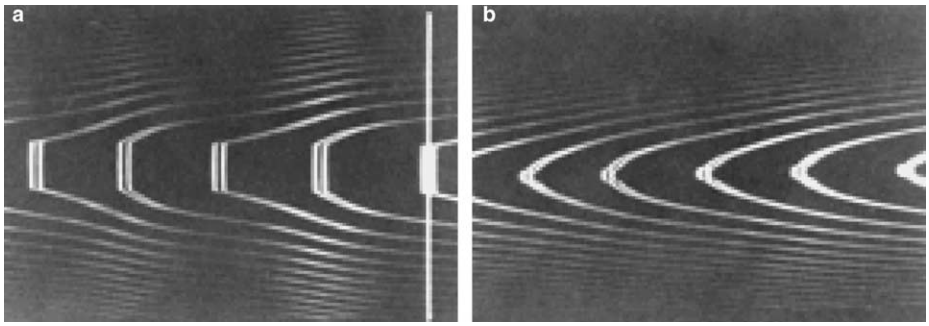

Fig. 4. Interferometry in SFA. FECO fringes when the surfaces are (a) in contact, and (b) separated. The separation distances between the samples can be obtained by measuring the wavelengths of the fringes. (Reproduced from Ref. [64] with permission by Applied Maths SFA Laboratory, ANU, Australia.)

fields to study shearing and friction forces, as well by laterally moving the mica sheets. This technique has contributed to the deeper understanding of the surface forces acting between micas [65], polymer surfaces [66,67], Langmuir–Blodget deposition [68,69], metal surfaces [70,71], refractive index measurement [72,73], protein adsorption [74], interfacial friction [75,76], viscosity [76–84], etc.

1.2.4. Atomic force microscopy

A very popular and versatile surface force measuring technique is the atomic force microscope (AFM), which was invented originally for surface imaging [19,20]. An AFM apparatus consists of four major components: cantilever deflection sensor, feedback mechanism for the positioner, piezoelectric micropositioner, and a cantilever-mounted tip (Fig. 5). According to the measurement modes, the AFM can be operated in contact, tapping, force modulation, and electric force mode. Detailed descriptions of these operating approaches can be found in the literature [21,85]. However, for our purposes essential is the measurement of the so-called force–distance curves. Since the AFM measures forces and displacements with high accuracy in the range of 10^{-13}–10^{-8} N and 0.1 Å [86], respectively, it can be used as a ''surface forces apparatus''.

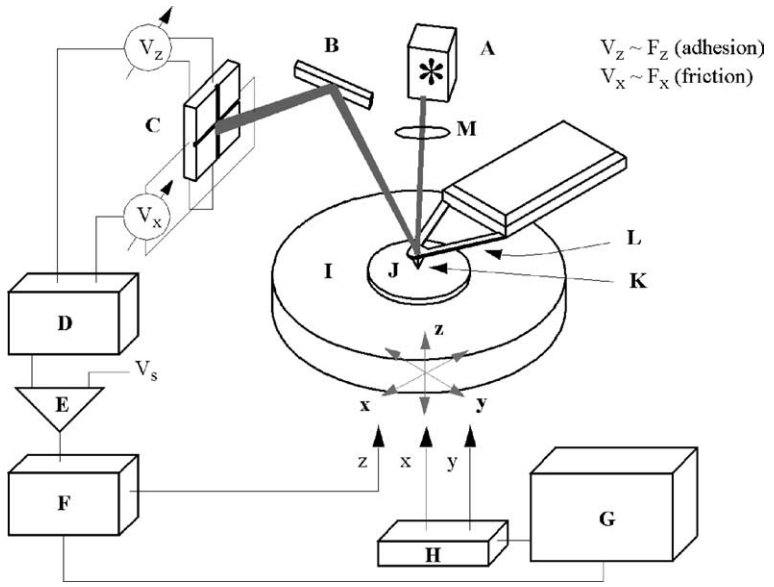

Fig. 5. Major components of an AFM apparatus: (1) cantilever deflection sensor: laser diode (A), mirror (B), 4-point photodetector (C); (2) feedback mechanism: divider/amplifier (D), differential amplifier (E), integrator (F), CPU and monitor (G), x–y translator (H); (3) piezoelectric micropositioner (I), sample (J); (4) cantilever mounted tip: cantilever (L), tip (K), and focusing lens (M).

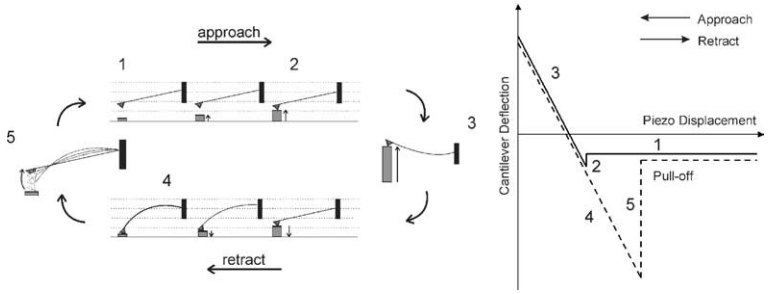

Fig. 6. Typical force–displacement curve for an AFM approach–withdrawal cycle [93].

The adhesion forces are studied by the analysis of the force–distance curves captured during the approach and the retraction of the sample with respect to the tip (Fig. 6). The measured value of the pull-off force, F_{ad}, (or adhesion force) is related to the work of adherence by either the DMT [87] or the JKR theory [14]. The DMT theory gives the following relationship between the pull-off force F_{ad} and the work of adhesion W:

$$F_{ad} = -2\pi RW \tag{17}$$

where R is the radius of the tip. The DMT approach is used when finite range forces, no deformation, and zero contact area in the moment of tip and sample separation are assumed. In practice, the adhesion force is usually calculated by the JKR theory of contact mechanics [14] since the surface profile and contact area of the contacting surfaces are better described. The JKR pull of force F_{ad} is given as:

$$F_{ad} = -\frac{3}{2}\pi RW \tag{18}$$

The contact radius a at pull-off in the JKR approach is defined by:

$$a = \left(\frac{1.2\pi R^2 W}{K}\right)^{1/3} \tag{19}$$

where K is the effective elastic modulus of the contact and is given (with the respective moduli E and Poisson's ratio v) as:

$$\frac{1}{K} = \frac{3}{4}\left(\frac{1-v_{tip}^2}{E_{tip}} + \frac{1-v_{sample}^2}{E_{sample}}\right) \tag{20}$$

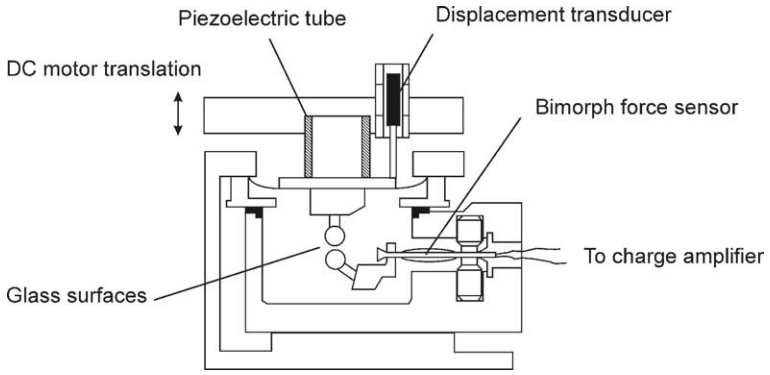

Fig. 7. Scheme of the MASIF apparatus. (Reprinted from [23], Copyright (2005), with permission from Elsevier.)

The estimation of the tip radius is crucial for the correct calculations, since it essentially affects the contact area between the tip and sample. Methods used to obtain the tip radius include inspection of electron microscope images of the tip [88], profiling of tips with sharp objects [89], or with colloidal gold clusters [90]. If colloidal spheres attached to cantilevers are used as probes, their radii can be known a priori [91,92].

Parallel with the development of AFM related surface force measurements, various techniques have emerged such as experiments in dry environment [94], in organic liquids [95–97], measurements of single molecular interaction forces [98], force titrations [99,100], and for monitoring chemical interaction by specific forces the so-called "chemical force microscopy" (CFM) [101–103]. Thus, by measuring surface forces the physical and chemical properties of a given surface can be mapped. Surface force measuring techniques can employ tips modified by alkanethiols [95,104,105], organosilanes [96,97], etc. to enhance chemically specific contrast. Modification can also be done by the attachment of a nanotube with a single reactive group on its end or a colloid particle in order to overcome the challenge of the undefined tip shape as mentioned before [91,92].

Using AFM, the force–distance curves obtained can be related to the surface properties in a fast manner. However, force–distance curves obtained are sometimes difficult to interpret due to the lack of exact knowledge of the contact geometry. The necessary calibration of the spring constant (k) of cantilevers may also have uncertainties, thus the obtained results must be interpreted with care.

1.2.5. Measurement and analysis of surface interaction force apparatus

The measurement and analysis of surface interaction force apparatus (MASIF) [22] resembles the SFA and the AFM approaches, as well. Similar to SFA, it utilizes large contact areas, thus it is more sensitive to surface roughness and contamination. As the approach is used to measure non-transparent materials, the apparatus is not equipped with contact area detection. Therefore, the direct determination of the surface separation is not possible. Similar to AFM, MASIF allows one to measure surface forces in a fast manner.

The MASIF utilizes a bimorph force sensor to obtain interaction forces between the materials of interest (Fig. 7) [23]. In this device the sample with one surface of interest is mounted on a piezoelectric tube and the other on the bimorph force sensor. The molecules of interest are deposited, or adsorbed, on glass spheres ($R \sim 1$–2 mm) [106], which are prepared by melting glass rods and flame polishing the spherical surfaces. During measurement the surfaces are brought into contact and separated again in a continuous manner. The coarse sample approach is carried out by a DC motor and the fine movements by a piezoelectric tube. The separation of the surfaces is calculated from the travel of the piezoelectric tube and from the deflection of the bimorph force sensor. A displacement transducer is used to directly monitor the displacement of the upper sphere sample. Contact is assumed when the displacement of the piezotube and the deflection of the force transducer are equal. The volume of the apparatus is rather small (10 ml). The MASIF apparatus was used to study polymers [23,107], interactions in emulsions [108], Langmuir–Blodget films [109,110], and sugar surfactants [111] with success among other things.

1.2.6. Adhesion-testing device (ATD)

To study the effects of surface forces, sensitive mechanical measurement techniques were developed before the 1970s [10,61,62]. Although the significance of surface force measurements was recognized, corresponding contact mechanics theories including adhesion had not been described at the time of construction of the first devices, i.e. the theory relating the observed deformation to the acting surface forces was inadequate. The existing, widely accepted theoretical approach was the Hertz

model which did not account for adhesion. In 1971 Johnson, Kendall, and Roberts worked out and published their milestone theory qualitatively describing contact mechanics [14]. In this paper it was shown that there is a finite contact area between surfaces under zero load. The external force required to separate two bodies of given surface energy and geometry in the presence of adhesion was also predicted. Johnson, Kendall, and Roberts were the first to find a relationship between surface force measurements (including adhesion) and Hertz's studies experimentally describing deformation of two elastic bodies in contact.

In the experiments studying JKR contact mechanics a lens-like elastic probe was brought into contact with a flat surface, while the applied external load (P), actual contact area (a), and the displacement (d) of the sample were recorded simultaneously and related to the JKR equation. However, there are some limitations of this adhesion-testing including that (i) one body has to be compliant, and (ii) one body has to be either transparent or opaque, which allows one to detect the contact area.

Later the apparatus and the measurement technique have been further developed to meet the challenges, such as employing different approaches for acquiring the experimental data (load, contact area, and displacement), using new data processing methods, excluding environmental effects, as well as applying elastomeric probes with shapes of cylinders [112], half cylinders split along their axes [113,114], cylinders having lens-like butt [115], cylindrical lens and a flat sheet [116], and a bended elastic ribbon "so-called" elastica loop [117].

The JKR-like experiments share a common basis and layout with the SFA. However, here, instead of determining the separation of the surfaces by the cumbersome optical interferometry, the changes of the contact area were simply detected by an optical microscope. The other difference is that the JKR-like experiments apply an elastomeric body (lens) and the adhesion is calculated from the contact area–external load data.

The early device used by JKR consisted of a lever arm system for the application of the external load. During the measurements the samples are brought into contact at zero load, then a negative load (overload) was applied through a micrometer screw connected directly to the mounting arrangements of one of the contacted surfaces [14]. The samples used were two equal rubber spheres with the diameter of 2.2 cm, as well as a rubber sphere and a rubber flat. The obtained contact radius and load data were fitted according to the JKR equation which is given as:

$$a^3 = \frac{R}{K}\left[P + 3\pi RW + \sqrt{6\pi RPW + (3\pi RW)^2}\right] \tag{21}$$

where a is the contact area, R is the radius of the lens, K is the combined elastic modulus (see Eq. (20)), and P is the external force.

A similar device was later used by Fuller and Tabor (Fig. 8) [118]. Their apparatus consisted of a cylindrical, lens-butted rubber specimen mounted on a spring arm, which was moved manually by a micrometer. The fine movement was carried out by another micrometer, which acted on a pivoted double lever system. The force was measured by an array of strain gauges mounted on the cantilever spring with an accuracy of 0.05 mN. The contact area was followed through the transparent specimen by an optical microscope. In the experiments the maximum force was measured which could be sustained by adhesion before separation.

Other adhesion-testing devices utilizing similar operation methods also emerged. Maugis and Barquins described their apparatus for studying adherence in 1978

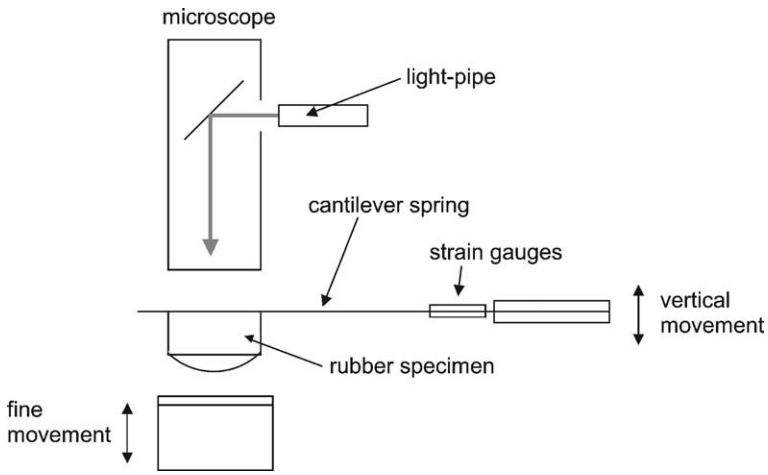

Fig. 8. Schematic of the adhesion-testing apparatus [118].

[115]. This instrument essentially encompassed a modified form of a device built for the study of rubber friction [119,120]. The measuring system consisted of a transparent glass hemisphere indenter and a flat elastomer sample. The load was applied to the lens, which was in the upper position, via a pivoting arm with the sensitivity of 10 mN and the displacement was measured with a precision of about 0.1 μm. The changes of the contact area were recorded by a camera, which was mounted on the top of an optical microscope. The contact radii were measured with the precision of about 1 μm at a magnification of 10×. For the adjustment of the center of contact and the optical axis the whole mechanical system could be shifted under the microscope.

Later, Chaudhury and Whitesides [121] introduced a further developed version of an adhesion-testing device, which utilized a pivoting arm. In their experiments interaction between a poly(dimethylsiloxane) (PDMS) lens and flat surfaces were studied in air. However, here the lower sample was placed onto the pivoting arm. The other end of the arm was attached to an electrobalance. The load was applied by translating the upper sample down (approaching) or up (retracting), while the actual force acting on the lever arm was determined by the electrobalance. The contact areas were recorded from beneath the samples by a camera. The device was also equipped with still photography.

Instruments based on the pivoting arm design are still in use, however the data acquisition and processing are continuously being updated [122–125].

In 1995, Deruelle and Tirrell published results obtained by a new adhesion-testing device, which utilized an analytical balance interfaced with a computer, an optical microscope and a manually operated, micrometer driven, translation stage [15]. A transparent elastomeric lens and a flat non-transparent substrate were used in these experiments, which were carried out stepwise with an average stabilizing time of 2 min. The contact area and the force were simultaneously measured. It is worth pointing out that this was the first description of a device where the axis of the acting force was in line with the axis of the load measurement, i.e. the length of the force arm did not play a role. The device was placed on an anti-vibration table at a later point [17,126].

Ahn and Shull [16] introduced their adhesion-testing apparatus and experimental protocol in 1996. The device consisted of an optical microscope, a force transducer, and a stepping motor for moving the transparent elastomeric lens or the flat substrate with the step size of 5.5 nm. Two different apparatus geometries were built including (i) standard device where the upper sample (transparent lens) was moved; (ii) inverted device where the lower sample (flat) was moved by a stepping motor. The authors placed the whole apparatus on a vibration isolation table that reduced the noise level to below ±0.05 mN. Furthermore, the acquired load and the contact area were captured and processed by a computer. The contact radii were obtained with an accuracy of ±2.3 μm. Experiments were performed in two ways: (i) quasi-equilibrium including stepwise application of the load, and waiting for a given period of time until equilibrium is reached i.e. no changes in the contact area was detected; (ii) dynamic measurement including continuous increase–decrease of the load. All experiments were conducted in ambient conditions. These versions of the adhesion-testing devices were soon developed further.

Shull et al. [127] designed and published an advanced apparatus, which had a fully linear, so-called axisymmetric layout (Fig. 9). The term axisymmetric refers to a layout, where all the parts, such as stepping motor, load transducer, samples and the image obtaining system were aligned along the same axis [127,128]. Thus, the unnecessary arm of the force that could act as a cantilever spring, bringing uncertainties in the data measured, was eliminated [129,130].

One of the most developed devices was built by Falsafi in the Tirrell group [18]. This JKR apparatus was the first, which unified most of the advances of the aforementioned

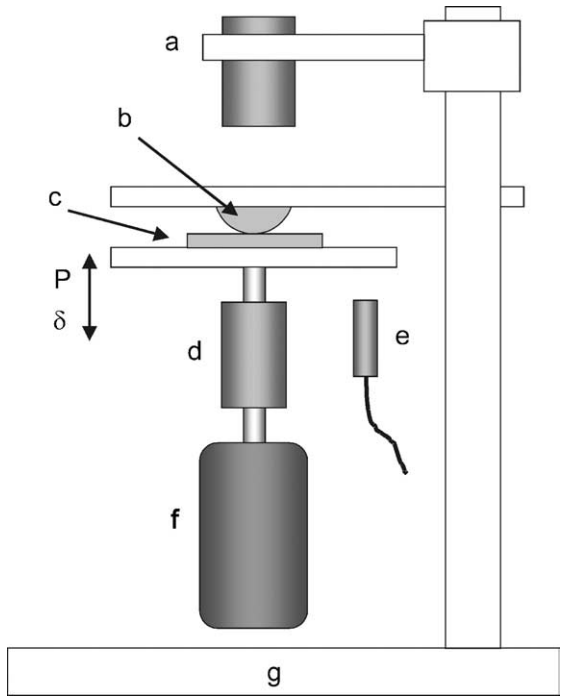

Fig. 9. Schematic representation of the experimental axisymmetric apparatus [129]. (a) Microscope, (b) elastomer lens, (c) polymer film, (e) displacement sensor, (f) linear stepping motor, (g) vibration isolation table. P and δ are the load and the indentation, respectively.

devices, however their setup was not axisymmetric. As a new innovation, a hot/cold stage was introduced around the samples. The temperature cell allowed measurements in the range of 0–250 °C with the precision of about ±0.05 °C. The whole device was put in an environmentally closed system, in which the levels of humidity could be controlled between 10% and 95% in a range of 10–40 °C. Thus by reducing the humidity the effect of capillary forces could be significantly reduced. Another new feature was the independent measurement of compression by a fotonic sensor, thus the value of displacement could be read directly during measurement with a resolution of about 20 nm. A CCD camera, which was mounted on a video zoom objective, was able to determine the contact areas with a resolution of 1 μm. All movements (motion resolution 50 nm), data acquisition and data treatment were controlled and carried out by a computer.

Based on the development of the apparatuses used in JKR-like adhesion measurement the following classifications can be made for the JKR ATD devices:

The geometry of the device:
- *traditional:* the imaging system is located at the top of the device,
- *upside-down:* the imaging system is located beneath the device (using inverted microscope).

Sample placement:
- *standard:* lens is above and flat substrate is beneath,
- *inverted:* lens is beneath the flat substrate.

Device operation:
- manual,
- *semiautomatic:* partly automated, either the data acquisition or hardware movement,
- *automatic:* all movements, the data acquisition and processing are controlled and operated by a computer.

Sample movement:
- straight movement usually along the vertical axis by means of a micrometer screw, linear motor, or stepper motor,
- *rotating movement:* pivoting arm, which can be either manually or electrically operated.

The operation modes of the devices can be divided into two main groups:
- dynamic measurement when the load is applied continuously,
- quasi equilibrium, or stepwise measurements.

1.3. Comparison of the surface force measurement techniques

The destructive techniques are not suitable to characterize the surface forces of solids materials. The main challenge to decouple superimposed thermodynamic work of adhesion and viscoelastic effects is still not reliably solved in the case of a general sample.

The contact angle measurement technique is one of the most accepted to characterize surface energetics. Although, this technique is used widely for the characterization of solid materials, the reliability of the results are questioned. The main advantage of this technique is that it can be performed easily and in a fast manner. Furthermore, it does not require expensive devices. IGC is only characterizing the γ^{d} of the material (powder) of interest, and this technique requires notable investment.

The other non-destructive surface force measuring techniques such as the SFA, MASIF, AFM, and JKR-like measurement techniques are based on rather expensive instruments and sometimes it can be a daunting task to perform measurements with them to obtain reliable quantitative data for surface forces. Table 1 lists the main differences between the SFA, MASIF, AFM and

Table 1
Comparison of the non-destructive surface force measuring instruments

	SFA	MASIF	AFM	JKR
Mode of operation	Stepwise or continuous	Continuous	Continuous	Stepwise or continuous
Samples	Transparent, molecularly smooth and flat over few hundreds of μm^2, uniform thickness	Spherical surfaces, molecularly smooth	Preferably hard, well-defined geometry	At least one opaque sample, smooth over few hundreds of μm^2, at elastomeric
Time scale of measurement	>Few minutes, <1 h except stepwise	0.1–2 min	0.001–0.001 s	>Few minutes, <1 h except stepwise
Determination of probe radius	Interferometry	SEM	SEM, profiling with sharp objects or gold colloids, colloidal probe	Optical microscopy
Data obtained from	Separation of surfaces vs. piezoposition	Bimorph deflection vs. piezoposition	Cantilever vs. piezoposition	Contact area vs. external load

JKR-like ATD techniques. As it can be seen, the special requirements of each measurement technique limit the possible ranges of samples. The time domain, the nature of the sample, and the shortcomings of measurements can help to decide which technique is recommended. So far, there is no undisputed surface force measuring technique of choice, therefore it is recommended to perform complementary measurements using different techniques.

In the subsequent section, in order to illustrate the use and the applications of JKR-ATD instruments, we describe the development, performance characteristics, and some selected applications of a custom-built device built in our laboratory.

2. Experimental

2.1. Sample preparation

As test specimens commercial poly(dimethylsiloxane) (PDMS) were used. Sylgard 184 (Dow Corning), consisting of PDMS and a reinforcing silica filler was prepared by carefully mixing the precursors Sylgard 184A/Sylgard 184B at a ratio of 10:1 by mass.[1] Sylgard 170 (Dow Corning), consisting of PDMS, a reinforcing silica filler and low amounts (<1 wt.%) of zinc oxide and carbon black was prepared by carefully mixing the precursors Sylgard 170A/Sylgard 170B at a ratio of 1:1 by mass. The mixtures were subsequently degassed in a vacuum oven at ambient temperature. For the JKR adhesion measurements films and sphere-cap-like lenses were prepared. For lens preparation small drops (1–2 μl) of the mixed and degassed precursors were applied with a microsyringe onto glass microscope slides, which had previously been treated with 1H, 1H, 2H, 2H perfluorodecyltrichlorosilane to reduce adhesion. The curing reaction was carried out at 120 °C for 24 h. The residual polymers and oligomers not covalently bound to the elastomer networks in the lenses were removed by subsequent Soxhlet extraction for at least 24 h using *n*-hexane as solvent, boiled at 120 °C. After extraction the lenses were dried in a vacuum oven at ambient temperature and stored in glass vials until use. Glass and silicon substrates were cleaned using Piranha solutions (mixture of 1:4 of 30% H_2O_2 and 70% concentrated H_2SO_4) at ambient temperature, carefully rinsed several times in Millipore water and ethanol, and finally dried in a stream of nitrogen gas. The PDMS precursors were then spin-coated onto the substrates using a Spincoater Model P6700 (Specialty Coating Systems Inc). After spin-coating the films were cured at 120 °C for 24 h and stored individually in plastic containers.[2] The thickness of the PDMS films ranged within 830 ± 100 nm as obtained by ellipsometry (a Plasmos SD 2002 ellipsometer was used at a wavelength of 632.8 nm at a fixed incident angle of 70°; the value of the refractive index n_f was assumed to be = 1.4). The flat substrates were used without extraction of the low molar mass siloxane fraction. For tensile testing 1 mm thick sheets of Sylgard 184 and 170 PDMSs were prepared using 1:10 and 1:1, 1:1.5 and 1:2 mixing ratios, respectively. The samples were cured at conditions similar to those used for the lenses and the flat substrates.

2.2. Adhesion-testing measurements

The measurements were performed by the ATD described in this paper in a continuous manner using 4 step s^{-1} ($\sim$10.2 mm min^{-1}) loading and unloading rates. The experiments were carried out at ambient conditions in an air conditioned room ($T = 20$ °C and RH = $\sim$30%).

2.3. Tensile test

Elastic moduli of the PDMS specimens were obtained by a Zwick Z020 tensile tester. The specimens were prepared by cutting ISO 37 T2 tensile testing bars out of $\sim$1 mm thick layers, which received the same treatments as the lenses prepared. The tensile samples were not subjected to extraction.

3. Results and discussion

3.1. Description and overview of the custom-built ATD

The scheme of the apparatus is illustrated in Fig. 10. The instrument is based on a stepper-motor operated, aluminium *XYZ* table. The resolution of the vertical movement (*z*-axis) is decreased to 42 nm by the application of a gearbox, which has a gear ratio of 30:1. The other two axes (also equipped with stepper motors) are not used in the current set up of the ATD. (Movements in the *x*–*y* plane are intended to employ performing special friction measurements in order to characterize the possible anisotropy of the surfaces.)

In traditional JKR-like adhesion experiments elastomeric lenses or an elastomeric lens and a hard substrate are pressed together along the vertical axis [15,16,65,114,115,118,129]. We call the contacting bodies as "lower" and "upper" sample, respectively. Using a similar layout, in our ATD the lower sample

[1] The PDMS networks of Sylgard 184 and Sylgard 170 are formed by a hydrosilylation reaction between vinyl-terminated oligomeric dimethylsiloxanes and a methylhydrosiloxane using a platinum complex as catalyst.

[2] The PDMS films on the silicon substrates were not extracted since this caused the films to delaminate from the substrates.

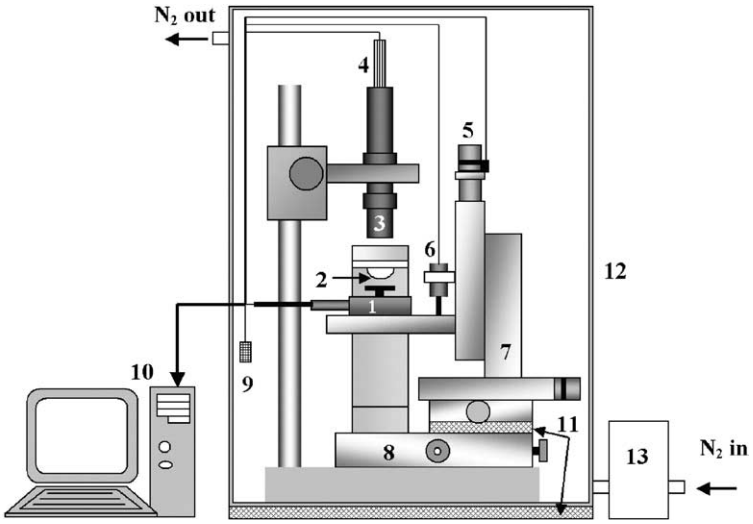

Fig. 10. The JKR device used to measure contact deformation between PDMS lenses and thin films. (1) Thin PDMS film substrates attached to the load cell. (2) PDMS lens. (3) Optical microscope. (4) CCD camera. (5) Stepper motor. (6) Displacement transducer. (7) *XYZ* table. (8) *XY* table. (9) Humidity and temperature sensor. (10) Computer. (11) Vibration damping rubber. (12) Glove box. (13) Humidity controller.

is placed on a table assembly shown in Fig. 10. This assembly consists of a steel table, which is attached to the mounting plate of the vertical slide of the *XYZ* table and also accommodates the subassembly of the force transducer. The force transducer, which is built in an aluminium block, can be equipped with custom-made sample holder tables. Depending on the shape of the lower sample two types of tables were used including (1) for attaching lenses the top part has a table-like shape, and (2) for attaching flat sample the top part has a threaded hole. For mounting these usually non-transparent flat samples a screw is glued (Pattex Uni-rapid, Henkel) in the centre of the back of each sample. The actual position and the movement of the lower-sample is monitored by a displacement transducer, which operates with a free-guided probe, targeted on the top surface of the steel table (Fig. 10(6)). Assuming rigid and stiff table assembly and very low deflection of the force transducer, measurements obtained with the geometry described and with the type of transducers used yielded results with sufficient accuracy. The holder assembly of the displacement transducer is attached to the non-moving part of the vertical slide of the *XYZ* table (Fig. 10).

The upper sample is placed on a transparent microscope slide, which is firmly fixed into the sample holder. The sample holder is clamped into a stand-alone rigid frame (Fig. 10). The applied clamp system gives the opportunity to change the samples in a fast and convenient manner. The attachment method of the upper sample also depends on the sample shape. Elastomeric lenses adhere well to the microscope glass. However, flat samples, which are spin-coated onto cover glasses, are usually fixed to the microscope glass slides using a transparent glue (Pattex Uni-rapid, Henkel). For good transparency and negligible effects on the overall stiffness, the hard glue must be applied in small amounts to form a very thin, bubble free and continuous layer.

During measurements the change of the contact area is monitored by a CCD camera. The camera is fixed on a 10× magnification, custom-built optical microscope, which is operated in reflection mode (Fig 10(3) and (4)). The sharpness of the camera image can be adjusted by the Olympus SZ-STS bonder arm. The maximum field of view is 535×414 μm. The light is coupled into the microscope via an optical fiber system. The intensity of the light can be adjusted manually, or for a similar effect the acquired video image can be digitally treated via the device operating program. The signal of the CCD camera is coupled into the host computer via an IMAQ 1408 image acquisition card.

The *XYZ* table is assembled onto a base plate which has three screws in order to level the lower part of the ATD. Small pieces of a vibration dumping rubber are applied under each screw to decrease the undesired resonation. The assembly of the *XYZ* table and the sample holder rest on a custom-made *XY* table (Fig. 8), which enables the operator to easily position the top of the lens inside the field of view before making contact with the sample. However, the visibility of the lens top is often obscured. The *XY* table, together with the upper sample holder and the *XYZ* table assembly, are placed on a stone base, which is equipped with a metal mounting post for holding the optical microscope.

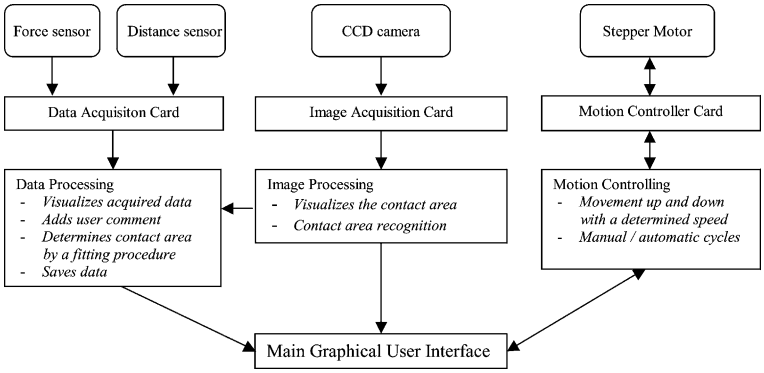

Fig. 11. Data flow diagram of the on-line data acquisition and device-operating program.

The well-defined conditions contribute to enhanced reproducibility of the measurements. As an improvement regarding environmental experimental conditions, the ATD was placed in an air-conditioned room. In order to further decrease the effect of environmental changes, the whole apparatus was put in a glove box (Fig. 10(12)). Relative humidity in the glovebox can be adjusted between 0% and 50% by means of controlled mixing of dry and wet streams of nitrogen. The actual temperature and the relative humidity is monitored inside the glovebox by a Sensiron SHT 11 sensor.

Another feature of the ATD is the Peltier-element based hot-stage, which can be attached to the upper sample holder. This accessory allows the user to perform temperature dependent experiments. However, in these experiments only the upper part of the sample is heated to avoid the undesired exposure of the force transducer to heat. Considering the location of the heating, a ring shaped heater element was applied to assure the visibility and the uniform temperature gradient of the contact area. The Peltier-element based heating device is calibrated between 20 and 140 °C.

The signals of the force and the displacement transducers are coupled into the host computer via an accessory board and a data acquisition card. The stepper motor is controlled through a so-called ValueMotion board and a stepper driver card. For data acquisition, treatment and device operation the host computer uses NI LabVIEW software by National Instruments. Both, the data acquisition and the operation of the stepper motor are processed and controlled by the same custom-made NI LabVIEW graphical user interface. According to the quality of the captured contact area images two ATD operating programs have been developed including (1) on-line edge detection for well defined contact areas, when continuous real time detection of the region of interest is possible, and (2) off-line edge detection: for obscured or non-continuous contact areas. In the latter case the program saves a series of images to disk for off-line manual analysis. Despite of the time consuming procedure, in some cases the image-by-image visual analysis proved to be the only way to accomplish the measurements. The flowchart of the principal operation of the automatic device-operating program is given in Fig. 11. The flowchart of the manual ATD operating program is similar, though it excludes the contact area fitting from the data processing and includes a time controller to set the sequence of the image and data saving procedures.

The data files saved consist of: (1) header including the time of the measurement, and the user comments given during measurements, and (2) the actual data consisting of the signal of the force transducer [V], signal of the displacement transducer [V], acquired pixel number [pix], global time [msec], temperature [°C], and humidity [%]. Data processing was done off-line, using a separate NI LabVIEW program.

3.2. Validation of the device with a compliant polymer

A validation of the data obtained was performed by the instrument is described below. As a straightforward and generally accepted method, adhesion measurements on a cross-linked poly(dimethylsiloxane) system were carried out [121,131]. The PDMS system has the advantage that its surface is smooth and well-defined, furthermore it is easy to prepare and is well-characterized. In order to understand the working principles of the numerical procedures used, a detailed description of the calculations will be given along with the results obtained.

Calculation of work of adhesion W and combined elastic modulus K. The data processing was done off-line, using a separate NI LabVIEW program. The data flow diagram summarizing the data treatment, the physical input parameters required and the fitting procedure are given in Fig. 12. The lens radius as a required parameter to perform the calculations was obtained separately by fitting procedures from a side view image of the lens captured by a 10× optical microscope.

The LabVIEW data processing program uses the JKR equation of contact mechanics to calculate the

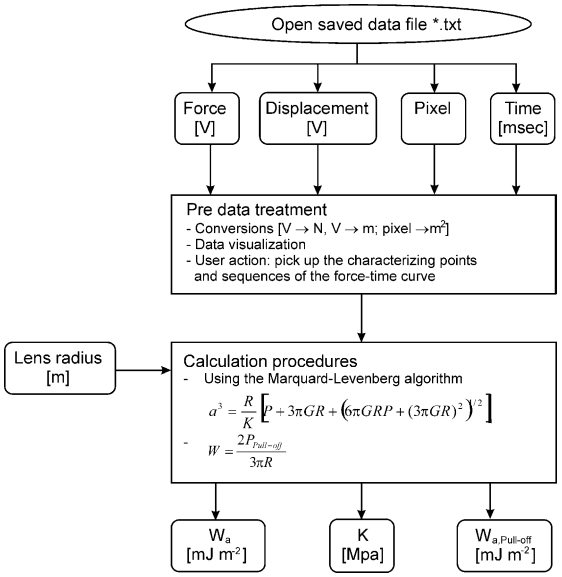

Fig. 12. Flowchart diagram of the JKR calculation program depicts the input data and shows the fitted output data, as well.

values of W, K and R, respectively. Although the program can fit all three parameters from the JKR equation, the result proved to be more correct if the value of the separately obtained lens radius was used as input and kept constant in the iterations. The calculation procedure utilizes the Levenberg–Marquardt algorithm [132,133] to determine the least squares set of coefficients that best fit the set of input data points (X, Y) as expressed by a non-linear function $y = f(x, a)$ where a is the set of coefficients. It must be mentioned that the pull-off force detected, just before the separation of the surfaces occurs, in some of the experiments was difficult to locate. Therefore the minimum point of the retraction curve (different from pull-off), the so-called maximum adherence force, is used to characterize the adhesive properties.

A typical loading–unloading cycle of a representative adhesion-testing measurement can be seen in Fig. 13, where the features of the curves are also depicted. In the plot the recorded force and acquired contact area are shown as a function of measurement time. Initially, before contact, the force transducer records the so-called "zero-force", i.e. the weight of the lower sample. The contact-area detecting procedure depends on the quality of the acquired image, therefore, in case of obscured video images it can detect zero or false (non-physical) areas. In the moment of the snap-on the top of the lens jumps into contact with the substrate generating a negative load on the force transducer and a detectable contact area. The loading part lasts until the motion is reversed. The maximum value of this point was determined according to McCullough et al. [124]. This method will be discussed in the section of elastic modulus determination. Upon retraction of the surfaces the unloading starts with a slowly descending curve. This region corresponds to the mechanical response of the device, namely the gearbox and the shaft. The unloading curve usually goes through a minimum (maximum adherence force), and ends with the sudden separation

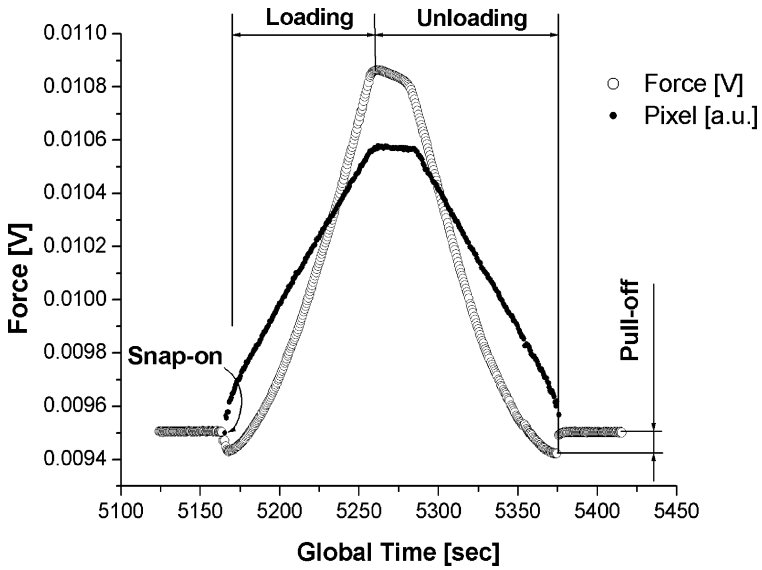

Fig. 13. A typical loading and unloading cycle of the PDMS sample system with the explanation of the characteristic features. Data of the force and contact area (pixel) are represented in real time of the measurement.

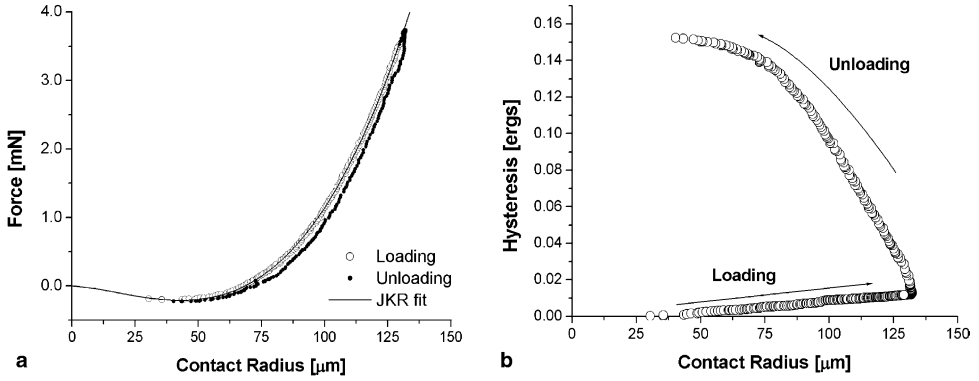

Fig. 14. (a) JKR fit to the advancing part of the loading–unloading cycle of the PDMS sample system. (b) The calculated cumulative adhesion hysteresis of the PDMS sample system.

(pull-off) of the surfaces. The last part of the cycle is the "zero force" (weight of the sample), where the surfaces are separated and far from each other.

Before running the JKR fitting procedure the recorded voltage signals of the transducers and the value of the pixel numbers are converted into the corresponding units (N and m). Furthermore, the above described regions (initial zero-force, loading curve, pull-off, final zero-force) are marked and separated for the calculations. A representative plot of the traditionally used force–contact curve with the JKR fit is given in Fig. 14a. As it can be seen the JKR fit follows well the advancing part of the loading–unloading cycle.

Calculation of adhesion hysteresis was also performed. The value of the adhesion hysteresis gives information (for PDMS) about the entanglement of tethered chains and their interdigitation with the extracted cross-linked PDMS network at the interface [134,135], as well as about the surface molecular relaxation effects. The calculated values of U_{adh} were small, indicating low interaction of the surfaces in contact (Table 3). In the plot, shown in Fig. 14b, the cumulative hysteresis is slightly increasing during loading. However, the increase is small, thus we can assume that the process is a quasi-equilibrium, when $G = W$.

Determination of elastic modulus (E) from contact mechanics data was also carried out. The value of the elastic modulus can be calculated from the JKR fit (Eq. (21)), or directly obtained from the experimental data using the measured displacements (i.e. the indentation data). The latter method can also be used to assess the validity of the parameters used to ensure elastic contact [124]. For practical reasons it is important to know that (1) the value of E of the elastomeric PDMS system is not constant at higher load values, and (2) the JKR equation is more sensitive to surface forces at lower external loads. As an alternative method to the JKR fit, the value of K can be determined by means of the measured displacements according to the following equations [14]:

$$\delta = \frac{a^2}{3R} + \frac{2P}{3aK} \tag{22}$$

Eq. (22) may be rearranged to give:

$$\left(\frac{3\delta}{a^2}\right) = \frac{1}{2} + \frac{2}{K}\left(\frac{P}{a^3}\right) \tag{23}$$

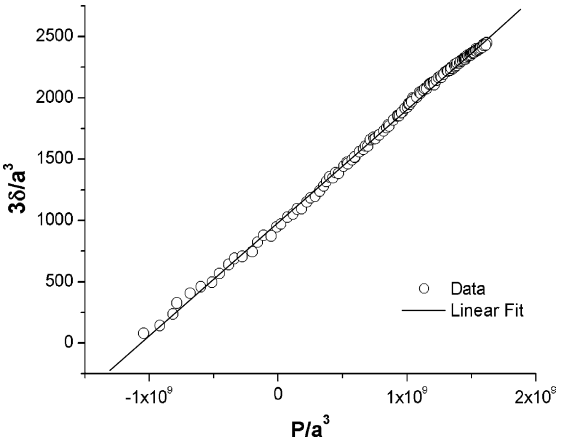

Fig. 15. The calculated elastic modulus from a loading–unloading cycle of the PDMS sample system.

Table 2
E moduli (tensile test) of the PDMSs used in the adhesion measurements

	Mixing ratios	E [MPa]
Sylgard 184	1:10	3.87 ± 0.61
	1:1	4.21 ± 0.24
Sylgaed 170	1:1.5	3.93 ± 0.19
	1:2	3.36 ± 0.25

The data was obtained on ISO 37 T2 tensile specimens. Mixing ratio is the ratio of the cross-linker to the base.

Table 3
Data analysis for different PDMS lens–substrate systems

PDMS system		W [mJ m^{-2}]	K [MPa]	γ [mJ m^{-2}]	U_{adh} [nJ]	E [MPa]	R [mm]
Lens	Substrate						
S185	S184	52.5 ± 1.3	1.99 ± 0.01	19.9 ± 1.9	–	–	–
S170	S184	43.0 ± 0.5	2.10 ± 0.01	21.5 ± 0.2	13.7 ± 0.9	3.1 ± 1.0	0.84 ± 0.25
S170	S170	42.0 ± 2.1	2.94 ± 0.08	22.7 ± 4.9	–	–	–

The JKR fit results were calculated with the separately obtained lens radii. Surface energies were determined from pull-off measurements. The values for U_{adh}, E and R were obtained only for Sylgard 170–184 system, using the above described methods.

Here, as earlier, the δ is the value of indentation, a is the contact area, K is the combined elastic modulus, and P is the applied load. Since the values of K and R are assumed to be constant in the applied load range of the measurements, a linear plot of $y = 3\delta/a^2$ vs. $x = P/a^3$ can be constructed with the slope of $2/K$ and intersection of $1/R$, respectively (Fig. 15). In particular, a higher external force can lead to a non-linear plot of the data. In the JKR calculation the non-linear behavior of the data can lead to erroneous results, therefore by using this plot the validity of the calculations can be verified.

The calculated values for the experimental data depicted in Fig. 15 $E = 2.2$ MPa, and $R = 1.02$ mm, respectively. The radius of the lens observed visually was 1.12 ± 0.02 mm and the value of E provided by the JKR fit was 1.2 MPa. The difference between the E moduli is 43%, which is consistent with previous experiments [136]. The results obtained suggest that the observed difference in values of E moduli is the result of the applied methods. The values of the E moduli obtained by tensile testing measurements on the Sylgard 184 and 170 PDMSs were in the order of the calculated values (Table 2). Although the value of the E modulus depends on the composition of the PDMSs, the annealing temperature has, as expected a significant influence, as well [137].

In the literature the surface free energy data of the PDMS has been determined and found between 20 and 26 mJ m^{-2}, however its mostly accepted value is 22 mJ m^{-2} [123,134,135,137,138]. The data obtained in our test measurements agree well for Sylgard 170 (Table 3). However, the values for the Sylgard 184 system is at the high end of the range. These higher values of W can be resulted by different surface roughness, or by different rates of diffusion of the low molar mass species to the surface following the extraction procedure.

4. Conclusions

The so-called JKR-like adhesion-testing measurement is a sensitive experimental method to directly obtain work of adhesion, interfacial surface free energy and surface free energy for solid materials. However, there are some limitations of this adhesion-testing method (1) one body has to be compliant, and (2) one body has to be either transparent or opaque, which allows one to detect the contact area detection.

An adhesion-testing device has been built and successfully tested as described. The instrument simultaneously records the applied force, displacement, acquired contact area, real time, humidity and temperature. The JKR theory of contact mechanics was applied to the experimental data to calculate work of adhesion, combined elastic modulus and lens radius. As a restriction of the fitting procedure, the radii of the elastomeric lenses were obtained separately and used throughout in the calculations. The device has been shown to be capable of accurately reproduce surface free energies of the PDMS model systems. The performance and throughput of the ATD has been significantly increased.

The measurements performed on PDMS model systems serve as validation and test of the ATD.

Acknowledgments

The authors gratefully acknowledge financial support from the Dutch Polymer Institute (project no: 182) (A.O.). Previous work and discussions with Dr. Jason Pickering, LabVIEW programming with Dr. Nikodem Tomczak, and help of Dr. Henrik Hillborg with specimen preparation are acknowledged.

References

[1] Tod DA. In: Packham DE, editor. Handbook of adhesion. Harlow: Longman Scientific & Technical; 1992. p. 470.
[2] Packham DE. In: Packham DE, editor. Handbook of adhesion. Harlow: Longman Scientific & Technical; 1992. p. 301.
[3] Zisman WA. In: Gould RE, editor. Contact angles, wettability, and adhesion. ACS Symp. Ser. 43. Los Angeles: ACS; 1964.
[4] Girifalco LA, Good RJ. J Phys Chem 1957;61(7):904–9.
[5] Good RJ, Girifalco LA. J Phys Chem 1960;64(5):561–5.
[6] Wu S. J Coll Interf Sci 1971;37(4):686.
[7] Wu S. J Polym Sci Part C 1971(34):19.

[8] Wu S. J Adhes 1973;5(1):39–55.
[9] Segeren LHGJ, Siebum B, Karssenberg FG, Pickering JP, van den Berg JWA, Vancso GJ. In: Mittal KL, editor. Particles on surfaces, vol. 7. Utrecht: VSB; 2002. p. 197–217.
[10] Tabor D, Winterton RHS. Proc R Soc Lond A 1969; 312(1511):435–50.
[11] Israelachvili JN, Tabor D. Proc R Soc Lond A 1972; 331(1584):19.
[12] Israelachvili JN, Adams GE. J Chem Soc Faraday Trans I 1978;74:975.
[13] Mangipudi VS. Intrinsic adhesion between polymer films: measurement of surface and interfacial energies. PhD thesis. University of Minnesota, 1995.
[14] Johnson KL, Kendall K, Roberts AD. Proc R Soc Lond A 1971;324(1558):301–13.
[15] Deruelle M, Leger L, Tirrell M. Macromolecules 1995; 28(22):7419–28.
[16] Ahn D, Shull KR. Macromolecules 1996;29(12):4381–90.
[17] Falsafi A, Deprez P, Bates FS, Tirrell M. J Rheol 1997;41(6):1349–64.
[18] Falsafi A. Contact mechanical measurement of block copolymer adhesion. PhD thesis. University of Minnesota, 1998.
[19] Binnig G, Rohrer H. Helv Phys Acta 1982;55(6):726–35.
[20] Binnig G, Quate CF. Phys Rev Lett 1986;56(9):930–3.
[21] Takano H, Kenseth JR, Wong SS, O'Brien JC, Porter MD. Chem Rev 1999;99(10):2845–90.
[22] Parker JL. Prog Surf Sci 1994;47(3):205–71.
[23] Claesson PM, Ederth T, Bergeron V, Rutland MW. Adv Coll Interf Sci 1996;67:119–83.
[24] Scheludko A. Adv Coll Interf Sci 1967;1:391–464.
[25] Exerowa D, Kolarov T, Khristov K. Coll Surf 1987; 22(2–4):171–85.
[26] Bergeron V, Radke CJ. Langmuir 1992;8(12):3020–6.
[27] Manev ED, Pugh RJ. Langmuir 1991;7(10):2253–60.
[28] Parsegian VA, Fuller N, Rand RP. Proc Natl Acad Sci USA 1979;76(6):2750–4.
[29] McIntosh TJ, Magid AD, Simons SA. Biophys J 1989; 55(5):897–904.
[30] Pezron I, Pezron E, Bergenståhl B, Claesson PM. J Phys Chem 1990;94(21):8255–61.
[31] Thomas RC, Houston JE, Crooks RM, Kim T, Michalske TA. J Am Chem Soc 1995;117(13):3830–4.
[32] Ashkin A, Dziedzic JM, Bjorkholm JE, Chu S. Opt Lett 1986;11(5):288–90.
[33] Kuo SC, Sheetz MP. Science 1993;260(5105):232–4.
[34] Svoboda K, Schmidt CP, Schapp BJ, Block SM. Nature 1993;365(6448):721–7.
[35] Perkins T, Smith DE, Chu S. Science 1994;264(5160): 819–22.
[36] Oláh A, Hillborg H, Vancso GJ. Appl Surf Sci 2004; 239(3–4):410–23.
[37] Oláh A. Contact mechanics of polymer interfaces: new approach in testing and control of adhesion. PhD thesis. Enschede: University of Twente; 2004 (ISBN 90 365 2105X).
[38] Cherry BW. Polymer surfaces. Cambridge: University Press; 1981.
[39] Andrews EH, Kinloch AJ. Proc R Soc Lond A 1973;332(1590):385–99.
[40] Irwin GR. J Appl Mech 1957;24:361–634.
[41] Griffith AA. Philos Trans R Soc Lond A 1920; 221:163–98.
[42] Owen MJ. Adv Chem Ser 1990;224:705–39.
[43] Good RJ. J Adhes 1972;4(2):133–54.
[44] Shanahan MER. In: Packham DE, editor. Handbook of adhesion. Harlow: Longman Scientific & Technical; 1992. p. 451.
[45] Berthelot D. Compt Rend 1898;126:1703.
[46] Packham DE. Int J Adhes Adhes 1996;16(2):121–8.
[47] Allen KW. J Phys 1993;3(C7):1511–6.
[48] Conder JR, Young CL. Physicochemical measurement by gas chromatography. Chichester: Wiley; 1979.
[49] Fowkes FM. In: Mittal KL, editor. Physicochemical aspects of polymers surfaces, vol. 2. New York: Plenum; 1981. p. 583.
[50] Fowkes FM. In: Mittal KL, Anderson HR, editors. Acid–base interactions: relevance to adhesion science and technology. Utrecht: VPS; 1991. p. 93.
[51] Schultz J, Lavielle L, Martin C. J Adhes 1987; 23(1):45–60.
[52] Dorris GM, Gray G. J Coll Interf Sci 1980;77(2):353–62.
[53] Drago RS, Wayland B. J Am Chem Soc 1965;87(16):3571.
[54] Gutmann V. The donor–acceptor approach to molecular interactions. New York: Plenum; 1978.
[55] Fekete E, Móczó J, Pukánszky B. J Coll Interf Sci 2004;269(1):143–52.
[56] Sun C, Berg JC. Adv Coll Interf Sci 2003;105(1–3): 151–75.
[57] Hamieh T, RageulLescouet M, Nardin M, Schultz J. Coll Surf A 1997;125(2–3):155–61.
[58] Schreiber HP. In: Akovali G, editor. The interfacial interactions in polymeric composites. Dordrecht: Kluwer; 1992.
[59] Comard MP, Calvet R, Dodds JA, Balard H. Powder Technol 2002;128(2–3):262–7.
[60] Segeren LHGJ, Wouters MEL, Bos M, van den Berg JWA, Vancso GJ. J Chromatogr A 2002;969(1–2):215–27.
[61] Derjaguin BV. Discus Faraday Soc 1954;18:24–41.
[62] Derjaguin BV. Quart Rev Chem Soc 1956;10(3):295.
[63] Israelachvili JN. Intermolecular and surface forces. 2nd ed. Academic press; 1991.
[64] Available from: http://wwwrsphysse.anu.edu.au/SFA/.
[65] Maugis D, Gauthier-Manuel B. J Adhes Sci Technol 1994;8(11):1311–22.
[66] Cho DL, Claesson PM, Gölander G-G, Johansson K. J Appl Polym Sci 1990;41(7–8):1373–90.
[67] Parker JL, Claesson PM, Wang JH, Yasuda HK. Langmuir 1994;10(8):2766–73.
[68] Kurihara K, Kunitake T, Higashi N, Nina M. Thin Solid Films 1992;210(1–2):681–4.
[69] Berndt P, Kurihara K, Kunitake T. Langmuir 1995; 11(8):3083–91.
[70] Parker JL, Christenson HK. J Chem Phys 1988; 88(12):8013–4.
[71] Levins JM, Vanderlick TK. J Phys Chem 1995; 99(14):5067–76.
[72] Kékicheff P, Spalla O. Langmuir 1994;10(5):1584–91.

[73] Curry JE, Christenson HK. Langmuir 1996; 12(23): 5729–35.
[74] Claesson PM, Blomberg E, Fröberg JC, Nylander T, Arnebrant T. Adv Coll Interf Sci 1995;57:161–227.
[75] Ohnishi S, Stewart AM. Langmuir 2002;18(16):6140–6.
[76] Israelachvili JN. J Coll Interf Sci 1986;110(1):263–71.
[77] Chan DYC, Horn RG. J Chem Phys 1985; 83(10):5311–24.
[78] Israelachvili JN, Kott SJ, Fetters LJ. J Polym Sci Phys 1989;27(3):489–502.
[79] Mate CM. Phys Rev Lett 1992;68(22):3323–6.
[80] McGuiggan PM, Zhang J, Hsu SM. Tribol Lett 2001;10(4):217–23.
[81] Granick S, Hu HW, Carson GA. Langmuir 1994;10(10):3867–73.
[82] Hu HW, Carson GA, Granick S. Phys Rev Lett 1991;66(21):2758–61.
[83] Homola AM, Nguyen HV, Hadziioannou G. J Chem Phys 1991;94(3):2346–51.
[84] Gee ML, McGuiggan PM, Israelachvili JN, Homola AM. J Chem Phys 1990;93(3):1895–906.
[85] Noy A, Vezenov DV, Lieber CM. Annu Rev Mater Sci 1997;27:381–421.
[86] Burnham NA, Colton RJ. In: Bonnell DA, editor. Scanning tunneling microscopy and spectroscopy. New York: VCH Publisher; 1993. p. 191.
[87] Derjaguin BV, Muller VM, Toporov YP. J Coll Interf Sci 1975;53(2):314–26.
[88] Noy A, Frisbie CD, Rozsnyai LF, Wrighton MS, Liebler CM. J Am Chem Soc 1995;117(30):7943–51.
[89] Griffith JE, Grigg DA, Vasile MJ, Russel PE, Fitzgerald EA. J Vac Sci Technol A 1992;10(4):674–9.
[90] Vesenka J, Manne S, Giberson R, Marsh T, Henderson E. Biophys J 1993;65(3):992–7.
[91] Ducker WA, Senden TJ, Pashley RM. Nature 1991;353(6341):239–41.
[92] Ducker WA, Senden TJ, Pashley RM. Langmuir 1992;8(7):1831–6.
[93] Schönherr H. From functional group ensembles to single molecules: scanning force microscopy of supramolecular and polymeric systems. PhD thesis. Enschede: University of Twente; 1999 (ISBN 90 365 13472).
[94] Thomas RC, Houston JE, Crooks RM, Kim T, Michalske TA. Am Chem Soc 1995;117(17):3830–4.
[95] Frisbie CD, Rozsnyai LF, Noy A, Wrighton MS, Lieber CM. Science 1994;265(5181):2071–4.
[96] Nakagawa T, Okagawa K, Kurumizawa T, Ozaki S. Jpn J Appl Phys 1993;32(2B):L239–96.
[97] Nakagawa T, Ogawa K, Kurumizawa T. J Vac Sci Technol B 1994;12(3):2215–8.
[98] Hoh JH, Cleveland JP, Prater CB, Revel J-P, Hansma PK. J Am Chem Soc 1992;114(12):4917–8.
[99] Vezenov DV, Noy A, Rozsnyai LF, Liebler CM. J Am Chem Soc 1997;119(8):2006–15.
[100] Chen Y, Wang L, He HX, Liu ZF. Mol Cryst Liq Cryst 1997;294:99–102.
[101] Green J-BD, McDermott MT, Porter MD. J Phys Chem 1996;100(32):13342–5.
[102] Werts MPL, van der Vegte EW, Hadziioannou G. Langmuir 1997;13(19):4939–42.
[103] Vancso GJ, Hillborg H, Schönherr H. Adv Polym Sci, 2005, in press.
[104] Thomas RC, Tangyunyong P, Houston JE, Michalske TA, Crooks RM. J Phys Chem 1994;98(17):4493–4.
[105] Green J-BD, McDermott MT, Porter MD, Siperko LM. J Phys Chem 1995;99(27):10960–5.
[106] Fröberg JC, Rojas OJ, Claesson PM. Int J Miner Process 1999;56(1–4):1–30.
[107] Schmitt FJ, Ederth T, Weidenhammer P, Claesson P, Jacobasch HJ. J Adhes Sci Technol 1999;13(1):79–96.
[108] Blomberg E, Claesson PM, Warnheim T. Coll Surf A—Physicochem Eng Asp 1999;159(1):149–57.
[109] Poptoshev E, Rutland MW, Claesson PM. Langmuir 2000;16(4):1987–92.
[110] Poptoshev E, Claesson PM. Langmuir 2002;18(4):1184–9.
[111] Kjellin URM, Claesson PM, Vulfson EN. Langmuir 2001;17(6):1941–9.
[112] Li LH, Tirrell M, Korba GA, Pocius AV. J Adhes 2001;76(4):307–34.
[113] Baney JM, Hui CY. J Adhes Sci Technol 1997; 11(3):393–406.
[114] Falsafi A, Tirrell M, Pocius AV. Langmuir 2000; 16(4):1816–24.
[115] Maugis D, Barquins M. J Phys D—Appl Phys 1978; 11(14):1989–2023.
[116] Chaudhury MK, Weaver T, Hui CY, Kramer EJ. J Appl Phys 1996;80(1):30–7.
[117] Qi J. Measurement of surface and interfacial energies between solid materials using an elastica loop. Masters thesis. Blacksburg: Faculty of Virginia Polytechnic Institute and State University; 2000. p. 159.
[118] Fuller KNG, Tabor D. Proc R Soc Lond A 1975; 345(1642):327–42.
[119] Barquins M, Courtel R. Wear 1975;32(2):133–50.
[120] Barquins M. J Adhes 1982;14:63–82.
[121] Chaudhury MK, Whitesides GM. Langmuir 1991;7(5): 1013–25.
[122] Chaudhury MK, Whitesides GM. Science 1992; 255(5049):1230–2.
[123] Silberzan P, Perutz S, Kramer EJ, Chaudhury MK. Langmuir 1994;10(7):2466–70.
[124] Chin P, McCullough RL, Wu WL. J Adhes 1997;64(1–4): 145–60.
[125] Ulman A, Choi GY, Shnidman Y, Zurawsky W. Isr J Chem 2000;40(2):107–21.
[126] Mangipudi VS, Huang E, Tirrell M, Pocius AV. Macromol Symp 1996;102:131–43.
[127] Shull KR, Ahn D, Chen WL, Flanigan CM, Crosby AJ. Macromol Chem Phys 1998;199(4):489–511.
[128] Mowery CL, Crosby AJ, Ahn D, Shull KR. Langmuir 1997;13(23):6101–7.
[129] Fabbroni EF, Shull KR, Hersam MC. J Polym Sci Pt B—Polym Phys 2001;39(24):3090–102.
[130] Crosby AJ, Shull KR, Lin YY, Hui CY. J Rheol 2002;46(1):273–94.
[131] Rundlöf M, Karlsson M, Wågberg L, Poptoshev E, Rutland M, Claesson P. J Coll Interf Sci 2000; 230(2):441–7.
[132] Levenberg K. Quart Appl Math 1944;2:164–8.
[133] Marquardt DW. J Soc Ind Appl Math 1963;11(2):431–41.

[134] Choi GY, Kim SJ, Ulman A. Langmuir 1997; 13(23):6333–8.
[135] Amouroux N, Leger L. Langmuir 2003;19(4):1396–401.
[136] Pickering JP. Materials science and technology of polymers. PhD thesis. Enschede: University of Twente; 2000 (ISBN:90 365 15653).
[137] Available from: http://zurich.ibm.com/st/microcontact/stamps/material.html.
[138] Perutz S, Kramer EJ, Baney J, Hui CY, Cohen C. J Polym Sci Pt B—Polym Phys 1998;36(12):2129–39.